The Heritability of Pathogen Traits - Definitions and Estimators

Venelin Mitov,*,[1,2] Tanja Stadler,[1,2]

[1]Department of Biosystems, Science and Engineering (D-BSSE)

[2]Swiss Federal Institute of Technology (ETH), Zürich, Switzerland

*Corresponding author: E-mail: venelin.mitov@bsse.ethz.ch

Associate Editor:

Abstract

Pathogen traits, such as the virulence of an infection, can vary significantly between patients. A major challenge is to measure the extent to which genetic differences between infecting strains explain the observed variation of the trait. This is quantified by the trait's broad-sense heritability, H^2. A recent discrepancy between estimates of the heritability of HIV-virulence has opened a debate on the estimators' accuracy. Here, we show that the discrepancy originates from model limitations and important lifecycle differences between sexually reproducing organisms and transmittable pathogens. In particular, current quantitative genetics methods, such as donor-recipient regression (DR) of surveyed serodiscordant couples and the phylogenetic mixed model (PMM), are prone to underestimate H^2, because they fail to model the gradual loss of phenotypic resemblance between transmission-related patients in the presence of within-host evolution. We explore two approaches correcting these errors: ANOVA on closest phylogenetic pairs (ANOVA-CPP) and the phylogenetic Ornstein-Uhlenbeck mixed model (POUMM). Empirical analyses reveal that at least 25% of the variation in HIV-virulence is explained by the virus genome both for European and African data. These results confirm the presence of significant factors for HIV virulence in the viral genotype and reject previous hypotheses of negligible viral influence. Beyond HIV, ANOVA-CPP is ideal for slowly evolving protozoa, bacteria and DNA-viruses, while POUMM suits rapidly mutating RNA-viruses, thus, enabling heritability estimation for a broad range of pathogens.

Key words: HIV, set-point viral load (spVL), donor-recipient regression, ANOVA, phylogenetic mixed model, Ornstein-Uhlenbeck

Article

Introduction

Pathogens transmitted between donor and recipient hosts are genetically related much like children are related to their parents through inherited genes. This analogy between transmission and biological reproduction has inspired the use of heritability (H^2) - a term borrowed from quantitative genetics (Falconer, 1996; Hartyl and Clark, 2007; Lynch and Walsh, 1998) to measure the contribution

32 of pathogen genetic factors to pathogen traits, such as virulence, transmissibility and drug-resistance of

33 infections.

34   Two families of methods enable estimating the heritability of a pathogen trait in the absence of

35 knowledge about its genetic basis:

36 • Resemblance estimators measuring the relative trait-similarity within groups of transmission-related

37   patients. Common methods of that kind are linear regression of donor-recipient pairs (DR) (Fraser

38   et al., 2014; Leventhal and Bonhoeffer, 2016) and analysis of variance (ANOVA) of patients linked by

39   (near-)identity of carried strains (Anderson et al., 2010; Shirreff et al., 2013).

40 • Phylogenetic comparative methods measuring the association between observed trait values from

41   patients and their (approximate) transmission tree inferred from carried pathogen sequences. Common

42   examples of such methods are the phylogenetic mixed model (PMM) (Housworth et al., 2004) and

43   Pagel's λ (Freckleton et al., 2002).

44 Most of these methods have been applied in studies of the viral contribution to virulence of an HIV

45 infection (Alizon et al., 2010; Bonhoeffer et al., 2015; Fraser et al., 2014; Hecht et al., 2010; Hodcroft

46 et al., 2014; Hollingsworth et al., 2010; Leventhal and Bonhoeffer, 2016; Lingappa et al., 2013; Shirreff

47 et al., 2013; Tang et al., 2004; van der Kuyl et al., 2010; Yue et al., 2013), quantified by $\log_{10}$ set

48 point viral load – lg(spVL) – the amount of virions per blood-volume stabilizing in HIV patients at

49 the beginning of the asymptomatic phase and best-predicting its duration (Mellors et al., 1996). In

50 the view of discrepant reports of lg(spVL)-heritability, several authors have questioned the methods'

51 accuracy (Fraser et al., 2014; Leventhal and Bonhoeffer, 2016; Shirreff et al., 2013). Shirreff et al. 2012

52 used simulation of trait-values on existing HIV transmission trees to reveal that phylogenetic comparative

53 methods report strongly under- or over- estimated values depending on the true heritability value used in

54 the simulation (Shirreff et al., 2013). Later, Fraser et al. 2014 claimed that DR is unbiased with respect to

55 lg(spVL)-heritability and is robust to trait-based selection for transmission (Fraser et al., 2014). Finally,

56 Leventhal and Bonhoeffer (2016) simulated Wright-Fisher generations of transmission confirming that DR

57 outperforms PMM in terms of robustness and accuracy and suggesting that current phylogenetic methods

58 are compromised by questionable assumptions, such as ultrametricity of trees (all measurements collected

59 at the same time) and neutral evolution of the trait. These three studies assume that once the trait value

60 is set in the recipient upon infection, it remains constant throughout its infectious time. This assumption

61 is partially acceptable for lg(spVL), see (Geskus et al., 2007) and references therein, but it is highly

62 arguable for pathogen traits in general, because mutations during infection are often associated with

63 phenotype changes, e.g. escape from adaptive immune response (Virgin *et al.*, 2009), drug resistance,

64 or thermotolerance (Dessau *et al.*, 2012; Presloid *et al.*, 2016). The theory of heritability, which was

65 developed by quantitative geneticists to study populations of animals and plants (Falconer, 1996; Hartyl

66 and Clark, 2007; Lynch and Walsh, 1998), does not account for individual gradual evolution and other

67 lifecycle differences between pathogens and mating species. This reveals the need for a careful transfer

68 of the quantitative genetics terminology and methods to the domain of pathogen traits.

69 In the section "Overview on heritability", we review the definitions of heritability for sexually

70 reproducing organisms and discuss how these definitions are affected by the lifecycle differences between

71 sexual species and pathogens. In the section "New Approaches", we uncover the reasons for biases

72 in current resemblance-based and phylogenetic estimators of heritability and explore two alternative

73 approaches to overcome these biases. In the Results section, we compare the different heritability

74 estimators using in-silico simulations of epidemics, and report a heritability analysis of spVL data from

75 a large HIV cohort. Our results allow to establish a lower bound for the viral genetic contribution

76 to set-point viral load. The Discussion section puts our modeling and empirical results into a broader

77 perspective.

78 **Overview on heritability**

79 Heritability in sexual species

80 Jacquard (1983) noticed that the term "heritability" has been used by quantitative geneticists to serve

81 three different concepts: (i) the genetic determination of a trait; (ii) the resemblance between relatives;

82 (iii) the efficiency of selection. Hence, it may be confusing to use the term "heritability" without an

83 accompanying definition or a qualifier like "narrow-sense", "broad-sense" and "realized". Below, we

84 briefly introduce this terminology; formal definitions are written in the section Materials and Methods.

85 *Genetic determination.* Considering a real-valued (quantitative) trait, the degree to which the genes

86 of individuals determine their trait-values is quantified in a statistical sense by the **broad-sense**

87 **heritability**, H^2. Assuming a sufficiently large population and full knowledge of the distinct genetic

88 variants (genotypes) influencing the trait, H^2 can be measured by the coefficient of determination, R^2_{adj},

89 obtained over a grouping of the population by genotype. In the world of animals and plants, though, it

90 is impossible to measure H^2 in this way, because population sizes are small compared to large numbers

91 of (usually unknown) genotypes. Thus, quantitative genetics focuses on estimating a lower bound for H^2

92 – the **narrow-sense heritability**, h^2. h^2 summarizes how much of the trait variance is attributable to

93 single-locus additive genetic effects and, in sexually reproducing populations, it can be estimated from

94 measures of the trait-resemblance between relatives.

95 *Resemblance between relatives.* Relatives resemble each other not only for carrying similar genes but also

96 for living in similar environments. Hence, it is necessary to disentangle the concept of resemblance from

97 that of genetic determination. For an ordered relationship such as parent-offspring, the resemblance is

98 usually measured by the **regression slope**, b, of expected offspring values on mean parental values. For

99 members of unordered relationships, such as identical twins, sibs and cousins, their relative resemblance

100 is quantified by the one-way analysis of variance (ANOVA), which estimates the so-called **intraclass**

101 **correlation** (ICC) denoted here as r_A[type of relationship].

102 *Efficiency of selection.* The last of the three concepts is that of the efficiency of selection for breeding

103 of the individuals with "best" trait-values. This is quantified by the **realized heritability**, h_R^2, defined

104 in Hartyl and Clark (2007) as the response to selection relative to the selection differential.

105 *Connecting the dots.* The success of quantitative genetics in the pre-genomic era relies on the insight that

106 *"inferences concerning the genetic basis of quantitative traits can be extracted from phenotypic measures*

107 *of the resemblance between relatives* (Lynch and Walsh, 1998)". Mathematically, this quote is expressed

108 as a set of approximations, which have become dogmatic in quantitative genetics:

$$H^2 = R_{adj}^2 \simeq r_A[\text{identical twins}]$$

109

$$h^2 \simeq b \simeq 4r_A[\text{half sibs}] \simeq h_R^2.$$

110 The first equation is valid in general, provided there is no strong maternal effect on the trait, the observed

111 twins have been separated at birth and raised in independent environments and the assumptions of

112 ANOVA such as normality and homoscedasticity are at least approximately met. The second equation,

113 though, is provable only for diploid sexually reproducing species. This is because genetic segregation and

114 recombination during sexual reproduction ensure that single-locus additive effects are inherited at bigger

115 proportions (1/2 from each parent) compared to multi-locus (epistatic) interactions (i.e. 1/4 for 2-loci-,

116 1/8 for 3-loci-interactions, etc) (Falconer, 1996; Lynch and Walsh, 1998).

117 In summary, in sexually reproducing populations, heritability is used to quantify to what extent the

118 genetics explain a trait (broad-sense heritability, H^2) as well as to measure or predict the response to

119 trait-based selection for reproduction (realized heritability, h_R^2). Since it is practically hard to measure H^2,

120 one often uses empirical measures of the resemblance between relatives (i.e. parent-offspring regression,

121 b, or ICC from half sibs, r_A) to estimate the extent, to which single-locus additive effects determine the

122 trait (narrow-sense heritability, h^2). It turns out that $h^2 \simeq h_R^2$, justifying the dual role of h^2 as a measure

123 of genetic determination and a measure for the rate of trait-evolution resulting from selection.

124 Transfer to pathogen traits

125 The transfer of the above terminology from traits of diploid organisms to pathogen traits is almost

126 verbatim and only requires substituting "pathogen genes" for "organism genes", "donor value" for

127 "parental value" and "recipient value" for "offspring value". However, three important differences between

128 the lifecycles of diploid organisms and pathogens alter the connections between the definitions and the

129 estimators:

130 • **Asexual haploid nature of pathogen transmission**

131 The first difference is that, unlike reproduction of diploid organisms, the transmission of a pathogen

132 from a donor to a recipient is more similar to asexual reproduction in haploid organisms, because,

133 typically, whole pathogens get transferred between hosts. Importantly, in the absence of genetic

134 segregation and recombination at transmission, there is no preference in transmitting single-locus

135 over multi-locus genetic effects.

136 • **Partial quasispecies transmission**

137 The second difference is that the transmitted proportion of genetic information characterizing the

138 pathogen in the donor is unknown and varying between transmission events. For example, for slowly

139 evolving bacteria such as *Micobacterium tubercolosis* (Mtb), transmission can be clonal (Bjorn-

140 Mortensen *et al.*, 2016), whereas, for rapidly evolving retroviruses like HIV, transmission is often

141 accompanied by bottlenecks causing only a tiny sample of the large and genetically diverse virus

142 population in the donor (aka quasispecies) to penetrate and survive in the recipient (Keele *et al.*,

143 2008).

144 • **Within-host pathogen evolution**

145 The third difference involves the change in phenotypic value due to within-host pathogen mutation and

146 recombination. While genetic change is rare during the lifetime of animals and plants and its phenotypic

147 effects are typically delayed to the offspring generations, it constitutes a hallmark in the lifecycle of

148 pathogens and causes a gradual or immediate phenotypic change such as increasing virulence, immune

149 escape or drug resistance.

150 For equal genotypes in donor and recipient as well as for distributions of donors and recipients being

151 equal to the total population distribution, the estimators b and r_A evaluated on transmission pairs would

152 be unbiased with respect to H^2. This has been shown in theory (Fraser *et al.*, 2014). Further, Leventhal

153 and Bonhoeffer (2016) showed through simulations that DR is accurate in the case of minute evolution

154 in the recipient host upon infection. In their simulation, partial quasispecies transmission and gradual
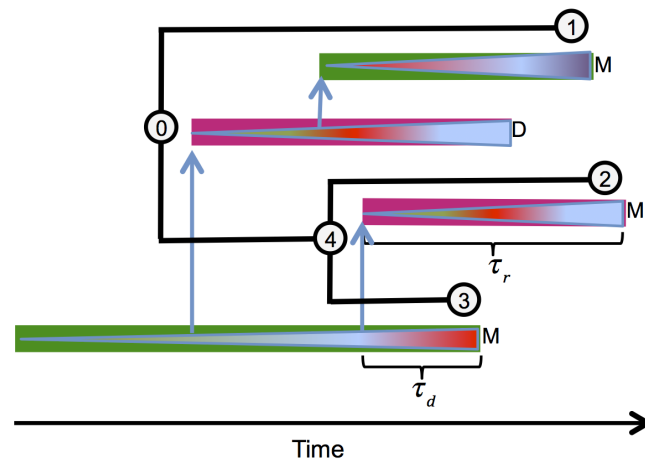
FIG. 1. A schematic representation of an epidemic. Colored rectangles represent infectious periods of hosts, different colors corresponding to different host types. Triangles inside hosts represent pathogen quasispecies, change of color indicating substitution of dominant strains. Capital letters denote host-events: M: phenotype measurement and recovery; D: host death. Vertical arrows show the time and direction of transmission events. The within-donor and within-recipient measurement delays, τ_d and τ_r, are shown for one donor-recipient couple. The transmission tree connecting the measured hosts is drawn

in black (shifted up-left for visualization purpose). Notice that, due to incomplete sampling, some infectious periods (colored rectangles) are shorter than their corresponding lineages on the tree. Couples of tips that are each other's closest tip by phylogenetic distance, e.g. (2,3), are called "phylogenetic pairs" (PPs). With some exceptions, PPs coincide with pairs of tips descending from the same parent node (a.k.a. siblings or "cherries").

155 within-host evolution throughout the infection is ignored. We notice, though, that these two phenomena

156 cause a negative bias in b and r_A as estimator of H^2, because they co-act for the loss of resemblance

157 without affecting H^2 in any way. Thus, b and r_A should be regarded as statistics summarizing the

158 resemblance in transmission couples observable after partial quasispecies transmission and delay between

159 transmission and measurements. Further in the text, we use the symbols b_τ and $r_{A,\tau}$ to emphasize that

160 these estimators have been calculated on a sample of donors and recipients with (variable) periods τ_d

161 and τ_r between transmission and measurements, $\tau = \tau_d + \tau_r$ denoting the total amount of time between

162 measurements (fig. 1). By contrast, we use b_0 and $r_{A,0}$ to emphasize that the calculation has been done

163 on the immediate trait-values right after transmission.

164 *Phylogenetic heritability.* As an alternative to resemblance-based methods, it is possible to fit a parametric

165 model of the trait-evolution along the branches of the transmission tree connecting the patients (fig. 1).

166 For example, the phylogenetic mixed model (PMM) (Housworth *et al.*, 2004; Lynch, 1991) assumes an

167 additive model of the trait-values, $z(t) = g(t) + e$, in which $z(t)$ represents the trait-value at time t for a

168 given lineage of the tree, $g(t)$ represents a heritable (genotypic) value at time t for this lineage and e

169 represents a non-heritable contribution representing the sum of cumulative environmental effects on the

170 trait and measurement error.

The PMM assumes that $g(t)$ evolves along the tree according to a branching Brownian motion process defined by the stochastic differential equation:

$$dg(t) = \sigma dW_t,$$
$$g(0) = g_0$$

(1)

where g_0 is the initial genotypic value at the root, W_t is the standard Wiener process and $\sigma > 0$ is the unit-time standard deviation (Grimmett and Stirzaker, 2001).

The environmental contribution e can change along the tree in any way as long as the values e at the tips are independent and identically distributed (i.i.d.) normal with mean 0 and variance σ_e^2. In the case of an epidemic, e represents the contribution from an individual's immune system; it obtains a value at the beginning of an infection, which can stay constant or change during the course of an infection, but is uncorrelated to the immune systems of other hosts. Denoting by $\bar{t}$ the mean root-tip distance in the tree, the **phylogenetic heritability** is defined as the expected proportion of phenotypic variance attributable to g at the tips:

$$H_{BM}^2 = \bar{t}\sigma^2 / (\bar{t}\sigma^2 + \sigma_e^2).$$

(2)

For rapidly evolving pathogens, such as RNA viruses, it is possible to infer the approximate transmission tree from pathogen sequences sampled at the moment of trait measurement (Hu *et al.*, 2004). This has inspired the use of PMM to estimate lg(spVL)-heritability in HIV patients (Alizon *et al.*, 2010; Hodcroft *et al.*, 2014; Shirreff *et al.*, 2013). However, this approach has been questioned in recent simulation tests reporting strongly positively or negatively biased PMM estimates with respect to the simulated H^2 (Leventhal and Bonhoeffer, 2016; Shirreff *et al.*, 2013).

Summary. In summary, for pathogen traits, measures of resemblance, such as b_0 and $r_{A,0}$, should be considered as estimates of H^2, compromised by quasispecies differences, rather than estimates of h^2. In the absence of genetic segregation and recombination at transmission, h^2 loses its dual role as an accessible measure of genetic determination and as a predictor for the rate of evolution. Due to delayed diagnosis, data from transmission couples for estimating b_0 and $r_{A,0}$ is rarely available in practice, while b_τ and $r_{A,\tau}$ are negatively biased due to gradual within-host evolution. Phylogenetic methods, such as PMM, should provide an alternative for estimating H^2 but recent simulation tests suggest that these methods are not well suited to the study of pathogen traits.

New Approaches

In this section, we first show through a real world example that the current methods, both resemblance-based and phylogenetic, are prone to strong negative bias in estimating H^2. As a principal cause, we reveal

197 the inability of these methods to model the gradual loss of phenotypic resemblance between transmission

198 related patients as a function of their phylogenetic distance. Then, we propose two alternative approaches

199 to account for this phenomenon. Finally, we design a toy model of an epidemic, which we use as a

200 validation tool for the different heritability estimators.

201 Uncovering biases in current heritability estimators

202 Previous studies of malaria and HIV have used clustering of the tips in the transmission tree to identify

203 donor-recipient couples (Hecht *et al.*, 2010; Hollingsworth *et al.*, 2010; Shirreff *et al.*, 2013) or groups

204 of transmission related patients (Anderson *et al.*, 2010). In particular, Shirreff *et al.* (2013) defines the

205 method of phylogenetic pairs (PP) as ANOVA on pairs of tips in the transmission tree that are mutually

206 nearest to each other by phylogenetic distance (τ) (fig. 1). Taking this approach a step further, we order

207 the PPs by τ and split them into bins of equal size, evaluating the correlation between pair trait-values

208 (r_A) in each bin. An analysis of 1912 PPs extracted from a recently published transmission tree of 8473

209 HIV patients (Hodcroft *et al.*, 2014) reveals a well pronounced decrease of the correlation between pair-

210 values (black points and vertical bars on fig. 2). For small τ (left-most bin), the correlation r_A is far

211 above the 95% CI estimated by the PP-method (thick grey horizontal bar), while, for big values of τ, r_A

212 falls below the 95% CI estimated by the PP-method. A similar pattern is observed when applying DR

213 (using b instead of r_A upon assigning a donor and a recipient at random in each phylogenetic pair; results

214 not shown). Being ignorant of τ, all resemblance-based methods average over τ in the observed sample

215 of pairs. Thus, these methods should be considered negatively biased in general. They can approximate

216 the true H^2 in the population only in the limit $\tau \to 0$ and up to additional sources of bias such as partial

217 quasispecies transmission and differences in the distributions of donors, recipients and total population.

218 Further, we repeatedly simulate trait-values on the transmission tree under the maximum likelihood

219 fit of the PMM method and re-evaluate the correlation in the same bins of PPs. Plotting the resulting

220 correlation estimates from the simulations next to the correlation in the original data shows that PMM

221 does not reproduce the gradual loss of correlation as a function of τ (brown points and vertical bars

222 on fig. 2). To understand the reason for that, we consider the initial assumption of the PMM method.

223 According to Brownian motion, the covariance between the values of a pair of tips (ij) is proportional

224 to the distance t_{ij} from the root to their most recent common ancestor (mrca):

$$\Sigma_{BM,ij} = \sigma^2 t_{ij}. \tag{3}$$

225 Without an additional requirement for ultrametricity of the tree (all tips at equal distance from the

226 root), this assumption does not imply a relationship between the covariance and the phylogenetic distance
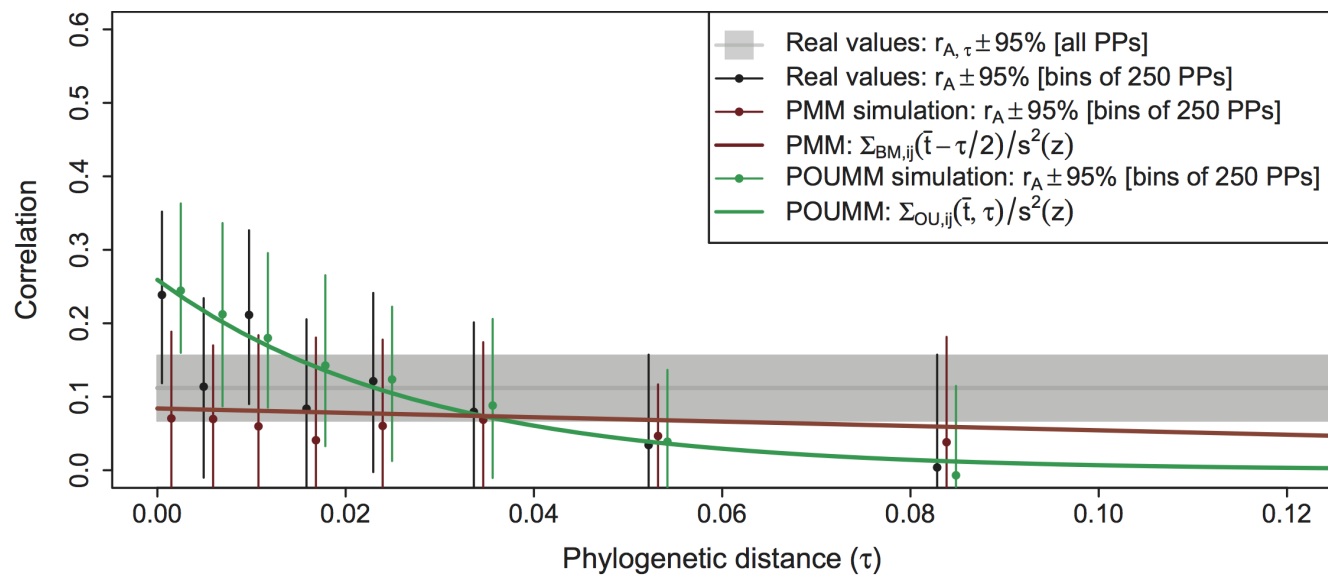
FIG. 2. Gradual loss of phenotypic resemblance between transmission related patients. A sample of PPs with real lg(spVL)-measurements from HIV patients shows a decrease in the correlation (ICC) between pair trait-values as a function of the pair phylogenetic distance τ. The PPs have been ordered according to τ and split into bins of 250 PPs (i.e. 500 patients). A thin and a thick grey horizontal bars denote the correlation with 95% CI in all PPs; black points with vertical bars denote the correlation with 95% CI within each bin. Brown and green points with vertical bars denote the mean correlation and 95% CI obtained after replacing the real trait values on the tree by values simulated under the maximum likelihood fit of the PMM and the POUMM methods respectively (mean and 95% CI estimated from 40 replications). A brown and a green line show the expected correlation between pairs of tips at distance τ as modeled by the PMM and the POUMM method: for PMM, this is the normalized covariance $\Sigma_{BM,ij}$ at the mean distance $\bar{t}-\tau/2$ from the root to the

pair's most recent common ancestor (eq. 3); for POUMM, this is the normalized covariance $\Sigma_{OU,ij}$ at the mean root-tip distance $\bar{t}$ and tip-pair distance τ (eq. 7). To approximate correlation, both covariances have been normalized by the total phenotypic variance, $s^2(z)$.

227   between the tips. In real non-ultrametric transmission trees, though, we observe a rapid loss of covariance

228   as τ increases, while there is only a weak relationship between covariance and root-mrca distance. The

229   latter is reflected also by a nearly horizontal slope of the expected covariance between PPs at distance τ

230   modeled under PMM as a function of their mean root-mrca distance ($\bar{t}-\tau/2$), $\bar{t}$ denoting the mean root-

231   tip distance (brown line on fig. 2). We conclude that the BM assumption is inappropriate for modeling the

232   evolution of pathogen traits along transmission trees. Instead, we need to model the covariance between

233   trait-values at the tips as a function of their phylogenetic distance.

234   New estimators of pathogen trait heritability

235   *ANOVA on closest PPs.* Assuming that the correlation measured in the bin at minimal τ is a more

236   accurate approximation of H^2 than the correlation in bins at bigger τ or the correlation of all PPs, we

237   refine the PP-method by imposing a limit on τ and define closest phylogenetic pairs (CPP) as PPs that

238   are not farther apart than a cut-off distance τ'. We tune this parameter based on the trade-off that arises

239   between the negative bias caused by τ and the loss of statistical power caused by omitting data. Further

240   in the text, we refer to this variant of the PP method as **ANOVA-CPP** with estimate $r_{A,\tau'}$. The main

241   drawback of this filtering technique is its reduced statistical power due to fewer observations.

242 *The phylogenetic Ornstein-Uhlenbeck mixed model.* The phylogenetic Ornstein-Uhlenbeck mixed model

243 (POUMM) is an extension of the PMM replacing the BM assumption with an assumption of an Ornstein-

244 Uhlenbeck (OU) process for the genotype evolution (Mitov and Stadler, 2017). The OU-process represents

245 a continuous time random walk, which tends to move around a long-term mean value with greater

246 attraction when the process is further away from that value (Uhlenbeck and Ornstein, 1930). Technically,

247 this is accomplished by adding an attraction term to eq. 1:

$$dg(t) = \underbrace{\alpha[\theta - g(t)]dt}_{\text{Attraction to } \theta} + \underbrace{\sigma dW_t}_{\text{Brownian motion}} , \tag{4}$$

248 where θ denotes the long-term mean and $\alpha > 0$ is the attraction strength. Since in the limit $\alpha \to 0$ the

249 attraction term vanishes and only the BM term remains, the OU-process represents a generalization of

250 BM. As in the PMM, a white noise is added to $g(t)$ at the tips. POUMM estimates the parameters of

251 the stochastic model and the white noise, and then evaluates the phylogenetic heritability as a function

252 of $\bar{t}$:

$$H_{OU}^2 = \frac{\sigma^2 \left(1 - e^{-2\alpha\bar{t}}\right)}{\sigma^2 \left(1 - e^{-2\alpha\bar{t}}\right) + 2\alpha\sigma_e^2}, \tag{5}$$

253 or as a time-independent function of the trait's sample variance, $s^2(z)$ (Mitov and Stadler, 2017):

$$H_e^2 = 1 - \sigma_e^2 / s^2(z). \tag{6}$$

254 Further in the text, we use the symbols H_{BMe}^2 and H_{OUe}^2 to denote the time-independent heritability (eq.

255 6) inferred respectively by PMM and POUMM.

256 The POUMM provides an interesting alternative to the PMM, since, under this model, the expectation

257 for the covariance between trait-values for a couple of tips (ij) is a function of both, their root-mrca

258 distance, t_{ij}, and their phylogenetic distance τ_{ij}:

$$\Sigma_{OU,(ij)} = \exp(-\alpha\tau_{ij})[1 - \exp(-2\alpha t_{ij})]\frac{\sigma^2}{2\alpha}. \tag{7}$$

259 As it turns out, data simulated under the maximum likelihood fit of the POUMM method reproduces the

260 loss of resemblance between PPs in the UK HIV data (green points and vertical bars on fig. 2). Plotting

261 the correlation between tips in the tree as expected by the OU-process (substituting $\bar{t}$ for t_{ij} in eq. 7

262 and normalizing by $s^2(z)$; green line on fig. 2) reveals that the correlation between transmission-related

263 patients decreases approximately exponentially with rate-constant equal to to the parameter α of the

264 OU process, ML estimate $\alpha = 36.3$, 95% CI [22.6, 62.4].

265 A toy-model of an epidemic

266 To test different estimators of heritability, we implement a phenomenological model of an epidemic, in

267 which an imaginary pathogen trait, z, is determined by the interaction between the alleles at a finite
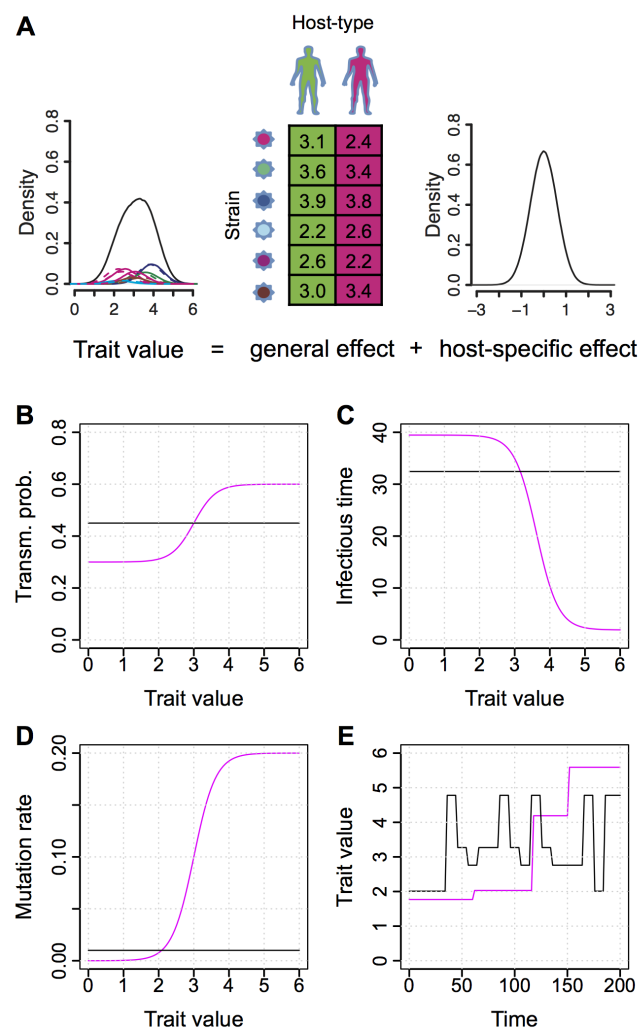
FIG. 3. A toy model of a pathogen trait with within-host evolution and SIR dynamics. (A) Schematic representation of a pathogen trait formed from a general ¡host type×carried strain¿ effect and a host-specific effect. The density of the trait-values in an infected population represents a mixture of normal densities corresponding to each one of twelve host type×strain combinations, scaled by their frequencies (dashed-lines depict host type 2); (B-E) SIR dynamics, color indicating selection modes with respect to to the trait-value, black: neutral, magenta: select (as specified in table 1); (B) Per risky contact transmission probability; (C) Expected infectious period if no mutation happens; (D) mutation rate (in mutations per site per time unit); (E) Example time-course of the trait evolution within a host; Time and trait-value units are arbitrary.

268 number of loci in the pathogen genotype and a finite number of immune system types encountered in

269 the susceptible population. This toy-model is embedded into a stochastic Susceptible-Infected-Recovered

270 (SIR) epidemic model (Keeling and Rohani, 2007), implementing "neutral" and "selection" modes of

271 within- and between-host dynamics. With the aid of figure 3, we briefly describe this model, leaving the

272 technical details for the section Materials and Methods.

273 We assume two equally frequent and lifelong immutable types of host immune system and two mutable

274 trait-determining loci in the pathogen genotype. With $M_1 = 3$ and $M_2 = 2$ possible alleles at each locus,

275 there are six possible genotypes denoted 1:11, 2:12, 3:21, 4:22, 5:31, 6:32 (fig. 3A). We assume absence

276 of strain coexistence within a host, so that the within-host quasispecies is represented by a single strain.

277 At a time t, the value $z_i(t)$ of an infected individual i is defined as a function of its immune system

type, $\mathbf{y}_i \in \{1,2\}$, the currently carried strain $\mathbf{x}_i(t) \in \{1,...,6\}$, and the individual's specific effect for this strain $e_i[\mathbf{x}_i(t)] \sim \mathcal{N}(0,0.36)$ drawn at random for each strain (in each infected individual). We call a (type $\mathbf{y}$-$\mathbf{x}$) **general effect** the expected trait value of type-$\mathbf{y}$ carriers of strain $\mathbf{x}$ in an infected population: $GE[\mathbf{y},\mathbf{x}] = \mathrm{E}[z|\mathbf{y},\mathbf{x}]$. For a set of fixed general effects, $z_i(t)$ is constructed according to the equation:

$$z_i(t) = GE[\mathbf{y}_i, \mathbf{x}_i(t)] + e_i[\mathbf{x}_i(t)] \tag{8}$$

We use a fixed set of general effects drawn from the uniform distribution $\mathcal{U}(2,4)$ for the twelve $\mathbf{y}$-$\mathbf{x}$ combinations (fig. 3A).

We embed this trait-model into a stochastic Susceptible-Infected-Recovered (SIR) model of an epidemic with demography and frequency dependent transmission as described in (Keeling and Rohani, 2007), ch. 1. Each infected individual, i, has a variable trait value $z_i(t)$ constructed as in eq. 8. Within-host phenomena (strain mutation and substitution) and between-host phenomena (natural birth, contact, transmission, diagnosis, recovery and death) occur at random according to Poisson processes. The rate parameters defining these processes are written in table 1.

For each group of parameters (within- and between-host), we consider the following two modes of dynamics:

- neutral: rates are defined as global constants mimicking neutrality (i.e. lack of selection) with respect to z (black lines on fig. 3B-D). For within-host phenomena, it is assumed that a mutation of the pathogen is followed by instantaneous substitution of the mutant for the current dominant strain, regardless of the induced change in z (black line on fig. 3E);

- select: borrowing the approach from (Fraser *et al.*, 2007), the rates of transmission and within-host pathogen mutation are defined as increasing Hill functions of 10^z, while the infected death rate is defined as an inverse decreasing Hill function of 10^z, thus mimicking increasing per capita transmission- and pathogen-induced mortality for higher z (red lines on fig. 3B-D). Within hosts, it is assumed that a mutation of the pathogen is followed by instantaneous substitution only if it resulted in a higher z. Otherwise, the mutation is considered deleterious (red line on fig. 3E).

By combining "neutral" and "select" dynamics for the strain mutation and substitution rates at the within-host level, and the virus-induced per capita death rate and per contact transmission probability at the between-host level, we define the following four scenarios (fig. 4):

- Within: neutral / Between: neutral;

Table 1. Within- and between-host dynamics of the toy epidemiological model.

Scope	Parameter	neutral	select
Between-host	Natural birth rate	$\lambda_{\mathrm{nat}} = 117.6$	
	Natural per capita death rate	$\delta_{\mathrm{nat}} = 1/850$	
	Per capita recovery rate	$\rho = 1/48$	
	Per capita contact rate	$\kappa \in \{\frac{1}{2}, \frac{1}{4}, \frac{1}{6}, \frac{1}{8}, \frac{1}{10}, \frac{1}{12}\}$	
	Per capita risky contact rate (S: current proportion of susceptible in the pop.)	$S \times \kappa$	
	Per risky contact transmission probability	$\gamma_{\mathrm{neutral}} = .45$	$\gamma(z) = \gamma_{\min} + \frac{(\gamma_{\max} - \gamma_{\min})(\gamma_{50})^{\gamma_{\mathrm{k}}}}{10^{z\,\gamma_{\mathrm{k}}} + (\gamma_{50})^{\gamma_{\mathrm{k}}}}$, where $\gamma_{\min} = .3, \gamma_{\max} = .6, \gamma_{50} = 10^3, \gamma_{\mathrm{k}} = 1.4$
	Per capita death rate for infected individuals	$\delta_{\mathrm{neutral}} = .01$	$\delta(z) = \delta_{\mathrm{nat}} + \frac{10^{z\,D_{\mathrm{k}}} + (D_{50})^{D_{\mathrm{k}}}}{D_{\min} 10^{z\,D_{\mathrm{k}}} + D_{\max} (D_{50})^{D_{\mathrm{k}}}}$, where $D_{\min} = 2, D_{\max} = 300, D_{50} = 10^3, D_{\mathrm{k}} = 1.4$
Within-host	Per locus pathogen mutation rate	$\nu_{\mathrm{neutral}} = .01$	$\nu(z) = \frac{\nu_{\max}(\nu_{50}) 10^{z\,\nu_{\mathrm{k}}}}{10^{z\,\nu_{\mathrm{k}}} + (\nu_{50})^{\nu_{\mathrm{k}}}}$, where $\nu_{\max} = .2, \nu_{50} = 10^3, \nu_{\mathrm{k}} = 1.4$
	Rate of substitution of strain $\mathbf{x}_j$ for $\mathbf{x}_i$, where $\mathbf{x}_i \neq \mathbf{x}_j$ at a single locus, l, M_l is the number of alleles at locus l, and the corresponding values are z_i and z_j	$\xi_l = \frac{\nu_{\mathrm{neutral}}}{M_l - 1}$	$\xi_{l,i \leftarrow j}(z_i, z_j) = \begin{cases} \frac{\nu(z_i)}{M_l - 1} & \text{if } \nu(z_i) < \nu(z_j) \\ 0 & ,\text{otherwise} \end{cases}$

307 ● Within: select / Between: neutral;

308 ● Within: neutral / Between: select;

309 ● Within: select / Between: select;

310 For each of these scenarios and mean contact interval $1/\kappa \in \{2, 4, 6, 8, 10, 12\}$ (arbitrary time units), we

311 perform ten simulations resulting in a total of $4 \times 6 \times 10 = 240$ simulations. In the next section, we discuss

312 the resulting heritability estimates from these simulations and from a real dataset.

313 **Results**

314 Simulations

315 Of 240 toy-model simulations, 175 resulted in epidemic outbreaks of at least 1,000 diagnosed individuals.

316 In each of these 175 simulations, we analyzed the population of the first up to 10,000 diagnosed

317 individuals. We denote this population by $Z_{10\mathrm{k}}$ and the corresponding transmission tree – by $T_{10\mathrm{k}}$.

318 The direct measure of broad-sense heritability, R^2_{adj}, was compared to the following estimators: b_0 in

319 all transmission couples found in Z_{10k}; b_τ in the same transmission couples; b_{D_1} in transmission couples

320 in Z_{10k} having τ not exceeding the first decile, D_1; $r_A[\text{id}]$ based on grouping by identity of carried strain

321 in Z_{10k}; $r_{A,\tau}$ based on phylogenetic pairs (PPs) in T_{10k}; r_{A,D_1} based on closest phylogenetic pairs (CPPs)

322 defined as PPs in T_{10k} having τ not exceeding the first decile, D_1, among all PPs; H^2_{BMe} and H^2_{OUe} based

323 on the maximum likelihood (ML) fit of the PMM and POUMM methods on T_{10k}. To calculate b_0, we

324 used the immediate trait-values at moments of transmission (usually not available in practice). All other

325 estimators were calculated using trait-values at the moment of diagnosis.

326 A detailed analysis of the different heritability estimates (table 2, fig. 4, Supplementary Notes,

327 supplementary figs. S1, S2, S3) confirmed the negative bias due to measurement delays in the resemblance-

328 based estimators b_τ and $r_{A,\tau}$. This bias was increasing with the mean contact interval, $1/\kappa$, because, for

329 a fixed recovery rate ρ, rarer transmission events resulted in longer transmission trees and, therefore,

330 longer average phylogenetic distance between tips, τ, (fig. S3). The negative bias was far less pronounced

331 when imposing a threshold on τ, but this came at the cost of statistical power (more accurate but longer

332 box-whisker plots for b_{D_1} and r_{A,D_1} compared to b_τ and $r_{A,\tau}$, fig. 4). Further, the simulations showed

333 that a worsening fit of the BM model on longer transmission trees caused an inflated estimate of the

334 environmental variance, σ^2_e, in the PMM method and, therefore, a negative bias in H^2_{BM} and H^2_{BMe}. As

335 explained in the previous section, this is caused by the inability of the BM assumption to model the loss of

336 phenotypic resemblance with increasing phylogenetic distance between tips. Several other sources of bias,

337 such as non-linear dependence of recipient on donor-values and deviation from normality were identified

338 and are summarized in table 3. We conclude that, apart from the practically inaccessible immediate

339 donor-recipient regression (b_0) and ICC of patients grouped by identity of carried strain ($r_A[\text{id}]$), the

340 most accurate estimator of H^2 in the toy-model simulations is H^2_{OUe} followed by estimators minimizing

341 measurement delays such as b_{D_1} and r_{A,D_1}.

342 Analysis of HIV-data

343 We performed ANOVA-CPP and POUMM on data from the UK HIV cohort comprising lg(spVL)

344 measurements and a tree of viral (pol) sequences from 8,483 patients inferred previously in (Hodcroft

345 et al., 2014). The goal was to test our conclusions on a real dataset and compare the H^2-estimates from

346 ANOVA-CPP and POUMM to previous PMM/ReML-estimates on exactly the same data (Hodcroft

347 et al., 2014). A scatter plot of the phylogenetic distances of tip-pairs against the absolute phenotypic

348 differences, $|\Delta \text{lg(spVL)}|$, reveals a small set of 116 PPs having $\tau \leqslant 10^{-4}$ while the phylogenetic distance

Table 2. Mean difference $\overline{\widehat{H^2} - H^2}$ from the toy-model simulations grouped by scenario. Statistical significance is estimated by Student's t-tests, p-values denoted by an asterisk as follows: * $p<0.01$; ** $p<0.001$. The column # denotes the number of simulations resulting in an epidemic outbreak under each scenario. Grey background indicates estimates that are unavailable in practice. Estimates of H^2_{OU} are not shown since they match with H^2_{OUe}.

Within/Between	#	b_0	b_{D_1}	b_τ	$r_A[id]$	r_{A,D_1}	$r_{A,\tau}$	H^2_{BM}	H^2_{BMe}	H^2_{OUe}
neutral/neutral	50	-0.01*	-0.07**	-0.25**	0.05**	-0.05**	-0.18**	-0.17**	-0.28**	-0.01
select/neutral	47	0.05**	0	-0.07**	0.08**	0	-0.06**	-0.01	-0.12**	0.01*
neutral/select	41	-0.02**	-0.04**	-0.2**	0.05**	-0.06**	-0.15**	-0.17**	-0.24**	-0.02**
select/select	37	0.04**	-0.01	-0.06**	0.06**	-0.03*	-0.08**	-0.04*	-0.16**	0.03**

349 in all remaining tip-pairs is more than an order of magnitude longer, i.e. $\tau > 10^{-3}$ (fig. 5A). A box-

350 plot graph of the trait-values along the tree shows that the range of trait-values is confined between 1

351 and 7 with relatively stable median and interquartile range (IQR) throughout the epidemic (fig. 5B).

352 This visual analysis of the data suggests that the distribution of trait values has been at equilibrium

353 during the time period covered by the transmission tree. The random distribution of the CPPs along

354 the transmission tree suggests that these phylogenetic pairs correspond to randomly occurring early

355 detections of infection (trait-values from each pair depicted as magenta segments on fig. 5B). Based on

356 the observed gap of τ, we defined these PPs as closest ones (CPP). We applied the $1.5 \times IQR$-rule on

357 $|\Delta \lg(\text{spVL})|$ to identify outliers among the CPPs. According to this rule, outliers are all CPPs having

358 absolute phenotypic difference below $Q_1 - 1.5 \times IQR$ or above $Q_3 + 1.5 \times IQR$, Q_1, where Q_3 denotes the

359 25th and 75th quantile of $|\Delta \lg(\text{spVL})|$ in CPPs and IQR denotes the interquartile range Q3-Q1. The

360 outlier CPPs defined in that way are shown as blue bullets on fig. 5.

361 We compared the following estimators of H^2, with and without inclusion of outlier CPPs in the data:

362 • ANOVA on CPPs/PPs;

363 • POUMM/PMM on the whole tree (including tips belonging to CPPs);

364 • POUMM/PMM on the tree obtained after dropping tips belonging to CPPs;

365 The results from these analyses are written in table 4. Excluding outlier CPPs, ANOVA-CPP (222

366 patients) reported lg(spVL)-heritability estimates of 0.31, 95% CI [0.19, 0.43]. POUMM (8,473 patients)

367 reported agreeing estimates of 0.25, 95% CI [0.16, 0.36] and 0.22, CI [0.13, 0.35] upon omitting all

368 222 patients belonging to CPPs. The slightly lower POUMM estimates could be explained by errors in

369 the transmission tree, which are not present in CPPs. These results show first, that ANOVA-CPP and

370 POUMM agree on disjoint subsets of the UK data and, second, that POUMM provides an alternative

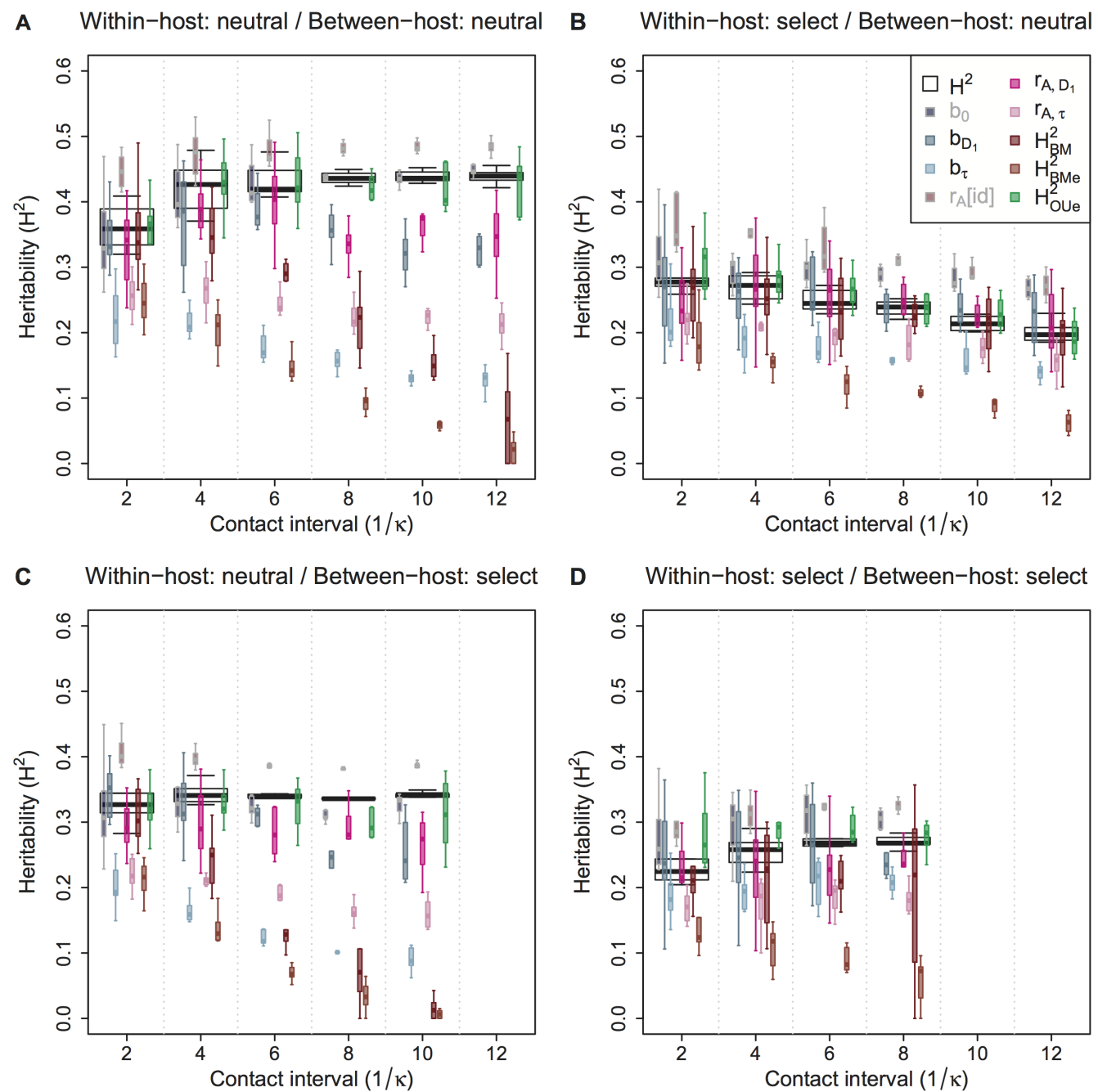371 to resemblance-based methods in the absence of early-diagnosed cases.

FIG. 4. Heritability estimates from computer simulations of the toy-model. (A-D) H^2-estimates in simulations of "neutral" and "select" within-/between-host dynamics. Each box-group summarizes simulations (first up to 10,000 diagnoses) at a fixed contact rate, κ; white boxes (background) denote true heritability, colored boxes denote estimates (foreground). Estimates that are not measurable in practice are shaded in grey. Statistical significance is evaluated through t-tests summarized in table 2. For an in-depth analysis of bias for fixed contact-rate κ, see Supplementary Notes, supplementary figs. S1 and S2. Estimates of H^2_{OU} are not shown since they match with H^2_{OUe}.

372   Figure 6 compares these estimates to previous lg(spVL) studies using phylogenetic and known

373   transmission-pairs data. In agreement with the toy-model simulations, estimates of H^2 using PMM or

374   other phylogenetic methods (i.e. Blomberg's K and Pagel's λ) are notably lower than all other estimates,

375   suggesting that these phylogenetic comparative methods underestimate H^2; resemblance-based estimates

376   are down-biased by measurement delays (compare early vs late on fig. 6).

Table 3. Sources of bias in estimators of H^2. The bias direction is indicated by a "+" or a "−", separated by a "/" when both directions are possible. The number of signs indicates the relative intensity of the bias that is observed in the simulations or in the analysis of the HIV data. A zero indicates no bias observed. A "?" indicates unknown direction. Horizontal lines separate sources that were identified in the SIR simulations (top) from sources identified in the analysis of the HIV data (middle) and sources suggested by this or previous works that were not tested (bottom). Grey background denotes estimators not available in practice.

Source of bias	b_0	b_{D_1}	b_τ	$r_A[id]$	r_{A,D_1}	$r_{A,\tau}$	H^2_{BM}	H^2_{BMe}	H^2_{OU}	H^2_{OUe}
Gradual within-host evolution	0	−	− −	0	−	− −	0	0	0	0
Violation of assumed model (i.e. BM)	0	0	0	0	0	0	+/− −	+/− −	+/−	+/−
Nonlinear dependence of expected recipient value on donor value	+/−	+/−	+/−	0	0	0	0	0	0	0
Non-normality of z	+/−	+/−	+/−	+/−	+/−	+/−	+/−	+/−	+/−	+/−
Loss of phylogenetic signal due to scarce transmission tree	0	0	0	0	0	0	+/−	+/−	+/−	+/−
Outliers in z	+/−	+/−	+/−	+/−	+/−	+/−	+/−	+/−	+/−	+/−
Partial quasi-species transmission	−	−	−	0	−	−	−	−	−	−
Temporal changes in the trait distribution	+/−	+/−	+/−	+/−	+/−	+/−	+/−	+/−	+/−	+/−
Outlying tips in the tree	0	0	0	+/−	+/−	+/−	+/−	+/−	+/−	+/−
Non-homogeneous evolutionary process	0	0	0	0	−	−	+/−	+/−	+/−	+/−
Random error in transmission tree	0	0	0	0	0	0	−	−	−	−
Biases in the transmission tree	0	0	0	0	?	?	?	?	?	?

377 In summary, POUMM and ANOVA-CPP yield agreeing estimates for H^2 in the UK data and these

378 estimates agree with DR-based estimates in datasets with short measurement delay (different African

379 countries and the Netherlands). Similar to the toy-model simulations, we notice a well-pronounced pattern
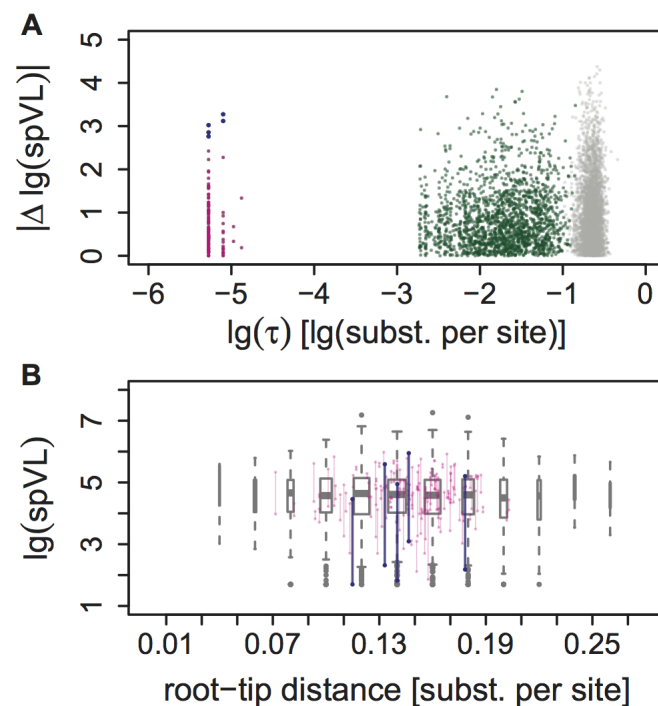
FIG. 5. Analysis of HIV-data from UK. (A) A scatter plot of the phylogenetic distances between pairs of tips against their absolute phenotypic differences: grey – random pairs; green – PPs ($\tau > 10^{-4}$); magenta: CPPs ($\tau \leqslant 10^{-4}$); blue – outlier CPPs (CPPs, for which $|\Delta \lg(\text{spVL})| > Q_3 + 1.5 \times (Q_3 - Q_1)$, Q_1 and Q_3 denoting the 25th and 75th quantile of $|\Delta \lg(\text{spVL})|$ among CPPs); (B) A box-plot representing the trait-distribution along the transmission tree. Each box-whisker represents the lg(spVL)-distribution of patients grouped by their distance from the root of the tree measured in substitutions per site. Wider boxes indicate groups bigger in size. Bullet-ending segments denote lg(spVL)-values in CPPs.

Table 4. ANOVA-CPP and POUMM estimates of lgspVL-heritability in HIV data from UK. Also written are the results from a previous analysis on the same dataset (Hodcroft et al. 2014). "=": the input data (and MCMC prior) is not altered by filtering out outlier CPPs; "–": the analysis was not done in the mentioned study. Grey background: estimates considered unreliable due to: a: negative bias caused measurement delays; b: negative bias caused by BM violation; c: presence of outlier CPPs;

Method	All tips in the phylogeny			Without outlier CPPs		
	N	$\hat{H}^2$	95% CI	N	$\hat{H}^2$	95% CI
ANOVA-CPP ($r_{A,10^{-4}}$)	232[c]	0.16[c]	[0.01, 0.30][c]	222	0.31	[0.19, 0.43]
ANOVA-PP ($r_{A,\tau}$)[a]	3834[a,c]	0.11[a,c]	[0.07,0.14][a,c]	3824[a]	0.11[a]	[0.08, 0.14][a]
POUMM (H^2_{OUe})	8483[c]	0.20[c]	[0.13,0.28][c]	8473	0.25	[0.16,0.36]
POUMM, no CPP (H^2_{OUe}; $\tau > 10^{-4}$)	8251	0.22	[0.13, 0.35]	=	=	=
PMM (H^2_{BMe})[b]	8483[b,c]	0.06[b,c]	[0.02, 0.09][b,c]	8473[b]	0.06[b]	[0.02, 0.10][b]
PMM, ReML (Hodcroft *et al.*, 2014)[b]	8483[b,c]	0.06[b,c]	[0.03, 0.09][b,c]	–	–	–

380 of negative bias for the other estimators, PMM and ANOVA-PP, as well as for the previous DR-studies
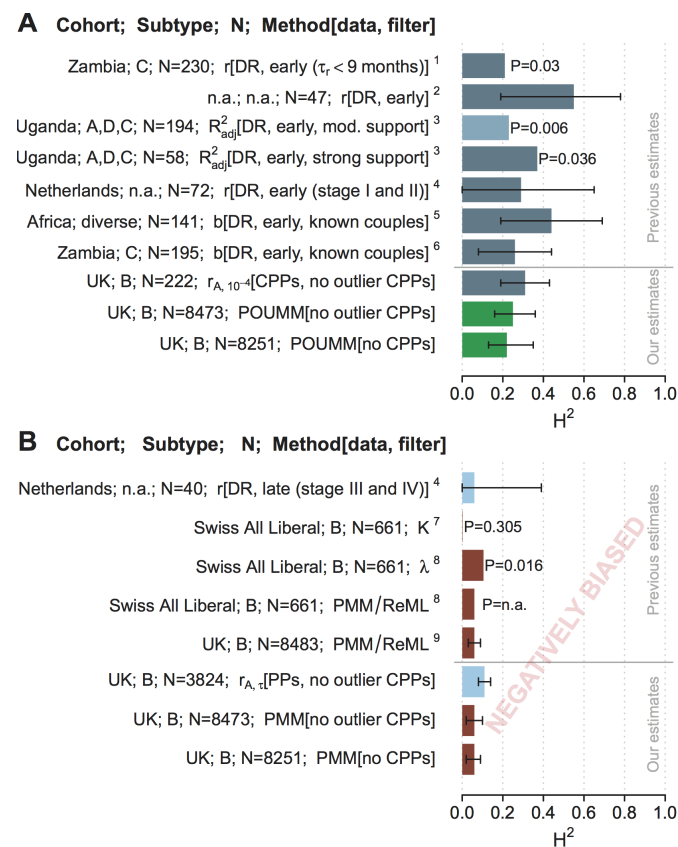
381 on data with long measurement delay.

FIG. 6. A comparison between H^2-estimates from the UK HIV-cohort and previous estimates on African, Swiss and Dutch data. (A) Estimates with minimized measurement delay (dark cadet-blue) and POUMM estimates (green); (B) Down-biased estimates due to higher measurement delays (light-blue) or violated BM-assumption (brown). Confidence is depicted either as segments indicating estimated 95% CI or P-values in cases of missing 95% CIs. References to the corresponding publications are written as numbers in superscript as follows: 1: Tang et al. 2004; 2: Hecht et al. 2010; 3: Hollingsworth et al. 2010; 4: Van der Kuyl et al. 2010; 5: Lingappa et al. 2013; 6: Yue et al. 2013; 7: Alizon et al. 2010; 8: Shirreff et al. 2013; 9: Hodcroft et al. 2014. For clarity, the figure does not include estimates from the UK data including the five outlier CPPs (table 4) and estimates from previous studies, which are not directly comparable (e.g. previous results from Swiss MSM/strict datasets (Alizon *et al.*, 2010)).

Discussion

Clarifying the terminology and notation

The first task of this study was the transfer of quantitative genetics terminology to the domain of pathogen traits. Due to important lifecycle differences between pathogens and mating organisms, it is essential to disentangle the concepts of relative resemblance and genetic determination. In essence, the estimators of trait resemblance between transmission-related patients, such as DR and ICC, and the phylogenetic heritability, must be regarded as lower bounds for the broad-sense heritability, H^2, compromised by partial quasispecies transmission, within-host evolution and various violations of model assumptions (table 3). A few examples from recent studies of HIV demonstrate the need for a careful consideration of these concepts. For example, in (Hodcroft *et al.*, 2014) and (Leventhal and Bonhoeffer, 2016) the authors introduce the PMM/ReML and the DR methods for estimating heritability after a definition of the narrow sense heritability, h^2. This can leave a confusing impression that the reported values are estimates of h^2 rather than H^2, because these methods are popular for estimating narrow-sense heritability for sexual

species. As another example, in (Fraser *et al.*, 2014; Shirreff *et al.*, 2013), the authors use the lower-case notation "h^2" to denote estimates of H^2. In fact, there are historical reasons to associate the symbol "h^2" with the regression slope, b (Fraser *et al.*, 2014; Wright, 1934). However, "h^2" is the standard symbol for narrow-sense heritability and b is, most of all, a measure of phenotypic resemblance. To avoid confusion, we recommend using the standard symbol "H^2" for broad-sense heritability (Hartyl and Clark, 2007; Lynch and Walsh, 1998) and different symbols for its indirect estimators.

A disagreement between simulation studies

Using simulations of a phenomenological epidemiological model, we have shown that two methods based on phenotypic and sequence data from patients - ANOVA-CPP and POUMM - provide more accurate heritability estimates compared to previous approaches like DR and PMM. However, we should not neglect the arising discrepancy between our and previous simulation reports advocating either PMM (Hodcroft *et al.*, 2014) or DR (Leventhal and Bonhoeffer, 2016) as unbiased heritability estimators. Compared to these simulations, the toy-model presented here has several important advantages: (i) it is biologically motivated by phenomena such as pathogen mutation during infection, transmission of entire pathogens instead of proportions of trait values, and within-/between-host selection; (ii) it is a fair test for all estimators of heritability, because it doesn't obey any of the estimators' assumptions, such as linearity of recipient- on donor values, normality of trait values, OU or BM evolution, independence between pathogen and host effects; (iii) it generates transmission trees that reflect the between-host dynamics, e.g. clades with higher trait-values exhibit denser branching in cases of between-host selection. As a criticism, we note that the toy-model does not allow strain coexistence within a host and, thus, is not able to model partial quasispecies transmission and, in particular, transmission bottlenecks (Keele *et al.*, 2008) or preferential transmission of founder strains (Lythgoe and Fraser, 2012). Although it may be exciting from a biological point of view, the inclusion of strain coexistence comes with a series of conceptual challenges, such as the definition of genotype and clonal identity, the formulation of the trait-value as a function of a quasispecies- instead of a single strain genotype, etc. These challenges should be addressed in future studies implementing more advanced models of within-host dynamics and leveraging deep sequencing data. To conclude, the discrepancy between simulation studies teaches that no method suits all simulation setups *ergo* biological contexts. Thus, rather than proving universality of a particular method, simulations should be used primarily to study how particular biologically relevant features affect the methods on table.

425 The heritability of HIV set-point viral load is at least 25%.

426 Applied to data from the UK, ANOVA-CPP and POUMM reported four to five times higher point

427 estimates and non-overlapping CIs compared to a previous PMM/ReML-based estimate on the same data

428 (0.06, 95% CI [0.02, 0.09]) (Hodcroft *et al.*, 2014). Our PMM implementation confirmed this estimate.

429 However, based on our simulations (fig. 2 and fig. 4), these estimates are still underestimates of the true

430 heritability. Overall, our analyses yield an unprecedented agreement between estimates of donor-recipient

431 resemblance and phylogenetic heritability in large European datasets and African cohorts, provided that

432 measurements with large delays have been filtered out prior to resemblance evaluation (Hecht *et al.*,

433 2010; Hollingsworth *et al.*, 2010) (fig. 6A). Also noteworthy is the fact that our estimates for the UK

434 dataset support the results from Fraser *et al.* (2014) who conducted a meta-analysis of three datasets on

435 known transmission partners (Hollingsworth *et al.*, 2010; Lingappa *et al.*, 2013; Yue *et al.*, 2013) (433

436 pairs in total) reporting heritability values of 0.33, CI [0.20,0.46]. All datasets support the hypothesis of

437 HIV influencing spVL ($H^2 > 0.25$). The particular estimates provided here should be interpreted as lower

438 bounds for H^2, because the partial quasispecies transmission, the noises in spVL measurements and

439 the noise in transmission trees are included implicitly as environmental (non-transmittable) effects. The

440 non-zero heritability motivates further HIV whole-genome sequencing (Metzner, 2016) and genome-wide

441 studies of the viral genetic association with viral load and virulence.

442 A critical view on the POUMM

443 The OU process has found previous applications as a model for stabilizing selection in macro-evolutionary

444 studies (Felsenstein, 1988; Hansen, 1997; Hansen and Bartoszek, 2012; LANDE, 1976) and references

445 therein. As a contribution of this work, we have shown that the OU process is well adapted for the

446 modeling of pathogen evolution along transmission trees in both, neutral as well as selection scenarios.

447 Unlike BM, OU models the phenotypic resemblance between transmission related patients as a function

448 of their phylogenetic distance, thus, capturing the gradual loss of resemblance caused by within-host

449 evolution (fig. 2). Most of the above-mentioned studies and the accompanying software packages have

450 assumed that the whole trait evolves according to an OU process, usually disregarding the presence of a

451 biologically relevant non-heritable component e or treating it as a measurement error whose variance is

452 a priori known (FitzJohn, 2012). Having the OU process act on the genotypic values rather than whole

453 trait-values is a simplifying assumption facilitating mathematical processing (Mitov and Stadler, 2017).

454 However, our toy model simulations have shown robustness and statistical power of the POUMM in

455 complicated scenarios combining trait-based selection at the within- and between-host levels. Another

456 criticism that can be addressed to the POUMM method is that it is unaware of between-host selection

and demographic processes, which may result in a correlation between tree structure and trait values (for example higher branching density in clades with higher z). As noted by Leventhal and Bonhoeffer (2016), this is a general issue with phylogenetic comparative approaches assuming a global evolutionary process acting on the whole phylogeny. An unexplored alternative would be to associate different instances of POUMM to different clades in the tree based on prior knowledge about heterogeneity between these clades.

Outlook

ANOVA-CPP and POUMM have great potential to become widely used tools in the study of pathogens. ANOVA-CPP works on pairs of trait values from carriers of nearly identical strains and can be easily extended to groups of variable size (Anderson *et al.*, 2010; Lynch and Walsh, 1998). Thus, ANOVA-CPP is ideal for slowly evolving pathogens such as DNA-viruses, bacteria and protozoa, where clusters of patients carrying identical-by-descent (IBD) strains are frequently found. For example, Anderson et al. 2010 identified 27 clusters of two to eight carriers of IBD strains in a small set of 185 malaria patients, i.e. 41% of the patients participated in clusters (Anderson *et al.*, 2010). On the other hand, IBD-pairs are rare for rapidly evolving RNA-viruses, such as HIV and HCV. For instance, we identified only 116 CPPs in a large dataset of 8483 HIV-sequences, i.e. less than 3% of the patients involved in IBD-pairs. However, the rapidly accumulating sequence diversity of RNA-viruses allows building large-scale phylogenies, which approximate transmission trees between patients. Thus, RNA-viruses should make the ideal scope for the POUMM. We believe that, together, the two methods should enable accurate and robust heritability estimation in a broad range of pathogens.

Materials and Methods

Formal definitions of heritability

Here, we briefly review the formal definitions of heritability in sexually reproducing populations based on the general linear model of quantitative traits (Falconer, 1996; Hartyl and Clark, 2007; Lynch and Walsh, 1998) and the three concepts introduced in the main text: the genetic determination of a trait, the resemblance between relatives, and the efficiency of selection.

The general linear model of a quantitative trait

A principal goal of quantitative genetics is to partition the observed phenotypic variance in a population into components attributable to genetic and environmental factors. Fundamental for the study of the genetic and environmental sources of variance is the general linear model for the phenotype (see Lynch and Walsh (1998), ch. 6), in which, for a given trait of interest, the observed phenotypic value, z, of an organism is represented as a sum of effects of the organism's genes, G, general (macro-) environmental

effects, E, gene by (macro-) environment interaction, I, and special (micro-) environmental effects e

$$z = G + I + E + e \tag{9}$$

It is assumed that the trait is influenced by a number of genes whose locations in the species' reference genetic sequence are called quantitative trait loci (QTL). In an individual, the configuration of alleles found at the trait's QTLs is called genotype and, for a population, the genotypic value, $G_{\mathbf{x}}$, of a genotype $\mathbf{x}$ is defined as the expected trait value of its carriers: $G_{\mathbf{x}} = \mathrm{E}(z|\text{genotype} = \mathbf{x})$. The remaining terms in eq. 9 are "defined in a least-squares sense as deviations from lower order expectations" (Lynch and Walsh, 1998). It is worthy to note that $G_{\mathbf{x}}$ depends on the distribution of $\mathbf{x}$ across environments in the population and that, by construction, the residuals $z - G = I + E + e$ have zero mean and are uncorrelated with G (Lynch and Walsh (1998), ch. 6). Thus, the total phenotypic variance observed in the population can be partitioned into a component that is purely genetic and a component that is attributable to both, non-genetic (purely environmental) factors as well as gene-by-environment interactions: $\sigma^2(z) = \sigma^2(G) + \sigma^2(z - G)$.

Measuring the genetic determination of a trait

Heritability in the broad sense, a.k.a. degree of genetic determination (Falconer, 1996), is defined as the ratio of the variance of genotypic values to total phenotypic variance in the population:

$$H^2 = \sigma^2(G)/\sigma^2(z) \tag{10}$$

A direct estimation of H^2 would require that all QTLs were known and that for each genotype there was a sample of measurements from individuals who were: (i) genetically identical at the QTLs; (ii) raised in randomly and independently assigned environments; (iii) present in the final dataset according to the population-specific environment-genotype frequencies. Given such a dataset of N independent measurements from carriers of all K distinct genotypes in the population ($K \ll N$), H^2 can be estimated by the ratio of sample variances $s^2(\hat{G})/s^2(z)$, where $\hat{G}$ denotes the individuals' genotypic values estimated by the mean value of their corresponding group and $s^2(\cdot)$ denotes sample variance. Though, intuitive, this formula is slightly positively biased in the case of finite sample size. Thus, we prefer its correction for finite degrees of freedom, a.k.a. as adjusted coefficient of determination:

$$R_{adj}^2 = 1 - \frac{N-1}{N-K} \frac{s^2(z - \hat{G})}{s^2(z)} \tag{11}$$

In the absence of full QTL information and data from independently grown clones, direct estimation of H^2 is rarely possible. Instead, quantitative geneticists focus on estimating its lower bound defined below.

515   **Heritability in the narrow sense** is defined as the ratio of variance of additive genetic values to

516   total phenotypic variance:

517

$$h^2 = \sigma^2(A)/\sigma^2(z) \tag{12}$$

518

519   The additive genetic value, A, of an organism is defined as the sum of additive effects of its alleles at

520   the trait's QTLs. We provide the technical definition of additive effect later on and note here that h^2

521   represents the largest proportion of phenotypic variance that can be explained by linear regression on

522   the allele contents at single QTLs, ignoring epistatic (inter-locus) and dominance interactions (Lynch

523   and Walsh, 1998). As discussed shortly, for sexually reproducing species, h^2 has two main advantages to

524   H^2: (i) it can be estimated from empirical data of genetically related (but not identical) organisms; (ii)

525   it can be used to predict the response to selection for traits associated with reproductive fitness.

Measuring the resemblance between relatives

527   Relatives resemble each other not only for carrying similar sets of alleles but also for living in similar

528   environments. Thus, it is necessary to disentangle the concept of resemblance from that of genetic

529   determination.

530   Considering an ordered relationship such as parent-offspring, the least squares regression slope of

531   offspring values on mean parental values is defined as

$$b = s(z_o, z_{mp})/s^2(z_{mp}) \tag{13}$$

532   where z_o and z_{mp} denote observed offspring and mean parent values, and $s(\cdot,\cdot)$ denotes sample covariance

533   among observed couples of values (Lynch and Walsh, 1998). Assuming no systematic dissimilarity between

534   parents and offspring, b is a value between 0 and 1, higher values indicating closer resemblance between

535   the expected phenotype of offspring and the mid-phenotype of their parents.

536   Considering members of unordered relationships, such as identical twins, sibs and cousins, the

537   resemblance between members within groups is measured by the intraclass correlation (ICC) defined

538   as the ratio of the "between group" variance over the total variance, $r_A = \sigma^2(c)/\sigma^2(z)$, c denoting the

539   observed within-group means (Fisher, 1925; Lynch and Walsh, 1998). Given a dataset of measurements

540   grouped by a factor such as twinship, the standard estimation procedure for r_A is the one-way analysis of

541   variance - ANOVA (see, e.g. (Donner, 1986) or ch. 18 in (Lynch and Walsh, 1998)). ANOVA uses mean

542   squares to find estimators for the between- and within-group variances, $\hat{\sigma}^2(c)$ and $\hat{\sigma}^2(z-c)$ and reports

ICC as the ratio:

$$r_A = \frac{\hat{\sigma}^2(c)}{\hat{\sigma}^2(c) + \hat{\sigma}^2(z-c)} \tag{14}$$

We notice that both, R^2_{adj} (eq. 11) and r_A (eq. 14), are estimators of ICC, but there is a key difference in their assumptions: R^2_{adj} assumes that all possible groups, i.e. genotypes, are present in the data but makes no explicit assumption about the distribution of group means (i.e. genotypic values); r_A is aware that only a subset of all possible groups is present in the data but assumes that the observed group means, are an i.i.d. sample from a normal distribution.

Measuring the efficiency of selection

In breeding experiments the goal is to optimize a trait by repetitive artificial selection for reproduction of the "best" individuals in a generation. A textbook example is truncation selection in which only individuals with measurements above a given threshold are allowed to reproduce. For a generation, the difference $\Delta_s = \mu_s - \mu$ between the mean value of individuals selected for reproduction, μ_s, and the mean of the generation, μ, is called the selection differential. Denoting by the mean of the offspring generation, the difference $R = \mu_o - \mu$, is called the response to selection. Then, the efficiency of the truncation selection is measured by the **realized heritability** (Hartyl and Clark, 2007), defined as the ratio:

$$h_R^2 = R/\Delta_s \tag{15}$$

Definition of additive genetic effect and additive genetic value

So far, we have skipped the more technical definition of additive genetic effect, which is the basis of the definitions of additive genetic value and narrow-sense heritability. Here we provide these definitions in the context of haploid organisms, noting that the definitions for diploid organisms found in textbooks (Falconer, 1996; Lynch and Walsh, 1998) are conceptually the same but somewhat more complicated for they treat dominance interactions separately from epistatic interactions.

We assume that a trait has a finite number of QTLs, L, with a finite number of alleles $M_l \geqslant 2$ for each locus $l = 1,...,L$. Denoting by x_{lm} the content (0 or 1) of allele m at locus l, $l = 1,...,L$, $m = 1,...,M_l$, we can describe an individual's genotype by a binary vector $\mathbf{x}$ of length $\sum_{1 \leqslant l \leqslant L} M_l$. The products of allele contents for different loci signify the presence or absence of allele combinations in a genotype. This representation results in the system of equations 16, in which the genotypic value of each genotype $\mathbf{x}$ is written as a sum of the population mean, μ, and the effects η_{lm}, $(\eta\eta)_{l_1 m_1 l_2 m_2}$ and so on, associated with each allele, couple of alleles at two loci and higher order- (up to order L) multi-locus configurations of alleles, present in the

genotype.

$$G_{\mathbf{x}} = \mu + \sum_{l \leq L} \sum_{m \leq M_l} \eta_{lm} x_{lm} + \sum_{l_1 \neq l_2} \sum_{\substack{m_1 \leq M_{l_1} \\ m_2 \leq M_{l_2}}} (\eta\eta)_{l_1 m_1 l_2 m_2} x_{l_1 m_1} x_{l_2 m_2} + ... \quad (16)$$

563 If for a moment we imagine that in system of equations $G_{\mathbf{x}}$, μ, and $\mathbf{x}$ are known while the $(\eta...)'$**s** are

564 unknown, from an algebraic point of view, there exist infinitely many combinations of $(\eta...)'$**s** solving the

565 system, because there are more unknowns than equations. From the point of view of genetics, however,

566 useful solutions are only those that maximize the proportion of variance in the genotypic values explained

567 by the effects of single alleles or low-order allele combinations. This reasoning finds a mathematical

568 reflection in the ordinary least squares (OLS) solution for the linear regression of $G_{\mathbf{x}}$ on single-locus

569 allele contents $\mathbf{x}$ (system 16 taken without the grey-shaded higher order terms on the right). Denoting

570 by $f_{\mathbf{x}}$ the frequency of genotype $\mathbf{x}$ among individuals in the population, the vector of OLS coefficients,

571 η^*, is found as a solution to the optimization task 17:

$$\eta^* = \arg\min_{\eta} \sum_{\mathbf{x}} f_{\mathbf{x}} (G_{\mathbf{x}} - \mu - \sum_{l \leq L} \sum_{m \leq M_l} \eta_{lm} x_{lm})^2 \quad (17)$$

572 The elements η^*_{lm} of any vector η^* solving this optimization task are called **additive allele effects**

573 and the sum $A_{\mathbf{x}} = \sum_{l \leq L} \sum_{m \leq M_l} \eta^*_{lm} x_{lm}$ is called **additive genetic value** of the genotype $\mathbf{x}$. As a detail, we

574 clarify that for multiple QTLs ($L > 1$) the vector η^* solving 17 is not uniquely defined because for each

575 locus one of the allele contents can be expressed as a function of the others, i.e. the design matrix of the

576 linear model is not of full rank. However the additive genetic values are invariant to the exact choice of

577 η^*.

578

Software

580 This study relies on the accompanying R-package "patherit". The used version of this package, together

581 with all program-code used for the toy-model simulations and the analysis of HIV-data, are provided

582 in the attached file SP.zip. Inside it, a file named ReadMe.txt contains further instructions on how to

583 run the code. The sub-sections below provide details on the implementation of the different heritability

584 estimators and the toy-model simulations.

585 *Direct measurement of H^2 in simulated data*

586 To measure H^2, we used the direct estimate R^2_{adj} (Eq. 11) after grouping the patients in the data by

587 their (currently carried) pathogen genotype and estimating the genotypic values as the group means

588 (implemented as function R2adj in the patherit package).

Calculating donor-recipient regression slope

590 The value of the donor-recipient regression slope (b_0, b_{D_1}, b_τ) was calculated using eq. 13, implemented

591 as a function called "b" in the patherit package.

Calculating r_A

593 To estimate r_A we implemented one-way ANOVA as a function "rA" in the package patherit. As a

594 reference we used the description in chapter 18 of (Lynch and Walsh, 1998). To calculate confidence

595 intervals, we used the R-package "boot" to perform 1,000-replicate bootstraps, upon which we called

596 the package function boot.ci() with type="basic". These confidence intervals were fully contained in the

597 standard ANOVA confidence intervals based on the F-distribution (see (Lynch and Walsh, 1998)), which

598 were slightly wider (not reported).

599

POUMM and PMM inference

601 The POUMM and PMM inference was based on an early version of the POUMM R-package (Mitov

602 and Stadler, 2017). Since the interface of the POUMM package has evolved considerably between the

603 version used in this analysis and the version 1.2.1 released on the Comprehensive R Archive Network

604 (CRAN, https://cran.r-project.org) at the time of writing this article. To facilitate reproducibility, the

605 source-code of the early version used in this analysis has been included in the accompanying package

606 'patherit'.

607 We performed maximum likelihood (ML) fits of the POUMM method in all toy model simulations. For

608 each simulated transmission tree, the conditional likelihood of the trait-values at the tips was maximized

609 over the parameters α, θ, σ, σ_e and g_0 (function ml.poumm of the patherit package). In the PMM ML

610 fits the conditional likelihood of the data was redefined as its corresponding limit for $\alpha \to 0$ and was

611 maximized over the parameters σ, σ_e and g_0 (ignoring θ, which cancels out in the case $\alpha \to 0$). To avoid

612 potential issues with floating point arithmetic all branch lengths were scaled-down 100 times before ML

613 fit. This preprocessing step is invariant with respect to the estimated heritability, since it only causes

614 rescaling of the OU parameters: $\sigma^2 \to \sigma^2 \times 100; \alpha \to \alpha \times 100$ (see eq. 5).

615 For HIV data, in addition to an ML-fit, we performed a Markov Chain Monte Carlo (MCMC)

616 fit (function mcmc.poumm of the patherit package) using an adaptive Metropolis algorithm with

617 coerced acceptance rate (Vihola, 2012) written in R (Scheidegger, 2012). The MCMC sampling was

618 performed on the POUMM parameters α, θ, σ^2 and σ_e^2. The prior was specified as a joint distribution

619 of four independent variables: $(\alpha, \theta, \sigma^2, \sigma_e^2) \sim \text{Exp}(0.01) \times \mathcal{U}(0,100) \times \text{Exp}(0, 10^{-4}) \times \text{Exp}(0.01)$. These low

620 exponential rates and the large interval of the uniform distribution were chosen such in order to ensure
621 that the prior is weakly informed, both, for the sampled parameters α, θ, σ^2, σ_e^2 and for the inferred
622 heritability estimates H_{OU}^2, H_{OUe}^2. This is verified by the nearly flat prior densities contrasting with
623 sharply peaked posterior densities (compare blue versus black curves on supplementary fig. S4 B). The
624 initial values for the parameters were set to $(\alpha, \theta, \sigma^2, \sigma_e^2)_0 = (0, 0, 1, 1)$. The adaptive Metropolis MCMC
625 was run for 4.2E+06 iterations, of which the first 2E+05 were used for warm-up and adaptation of the
626 jump distribution variance-covariance matrix. The target acceptance rate was set to 0.01 and the thinning
627 interval was set to 1,000. The convergence and mixing of the MCMC was validated by visual analysis
628 (supplementary fig. S4 A) as well as by comparison to a parallel MCMC-chain started from a different
629 initial state. The presence of signal in the data was confirmed by the observed difference between prior
630 (blue) and posterior (black) densities (see supplementary fig. S4 B). Calculation of 95% CI was done
631 using the function "HPDinterval" from the coda package (Plummer *et al.*, 2006).

632 *Computer simulations of the toy epidemiological model*

633 The toy-model SIR simulation is implemented in the function "simulateEpidemic" of the patherit package;
634 the extraction of diagnosed donor-recipient couples – in the function "extractDRCouples"; the extraction
635 of a transmission tree from diagnosed individuals – in the function "extractTree".

636 At the between-host level, the phenomena of birth, contact, transmission, recovery and death define
637 the dynamics between the compartments of susceptibles, infected and recovered individuals - X, Y and Z.
638 The natural birth rate, λ_{nat}, and the natural per capita death rate, δ_{nat}, are defined as constants satisfying
639 $\lambda_{\mathrm{nat}} = \delta_{\mathrm{nat}} N_0$, so that the average lifespan of an uninfected individual equals $1/\delta_{\mathrm{nat}} = 850$ (arbitrary) time
640 units and in a disease-free population the total number of alive individuals equilibrates at $N_0 = 10^5$. An
641 epidemic starts with the migration of an individual with random immune system type carrying pathogen
642 strain 1:11 to a fully susceptible population of N_0 individuals. Each individual has contacts with other
643 individuals occurring randomly at a constant rate, κ. A transmission can occur upon a contact involving
644 an infected and a susceptible individual, here, called a "risky" contact. It is assumed that the probability
645 of transmission per risky contact, γ, is either a constant (black on fig. 3B) or a function of the value
646 z (magenta on Fig. 3B) of the infected host and does not depend on the uninfected individual. Once
647 infected, a host starts transmitting its currently dominant pathogen strain at a rate defined as the product
648 of γ, κ, and the current proportion of susceptible individuals in the population, $S = X/N$. Thus, for fixed
649 κ, the transmission rate of an infected host is a function of the global variable S and the constant or
650 variable γ. This transmission process continues until recovery or death of the host. Recovery has the

651   meaning of a medical check occurring at a constant per capita rate, ρ, followed by immediate therapy

652   and immunity. Due to the virulence of the pathogen, an infected host has an increased (per capita) death

653   rate, δ, which is defined either as a constant or as a function of z. Based on their scope of action, we call

654   "between-host" the parameters λ_{nat}, δ_{nat}, κ, γ, ρ and δ.

655   Within a host, mutants of the dominant strain can appear at any time as a result of random single-

656   locus mutations, which occur at a constant or z-dependent rate, ν. It is important to make a distinction

657   between a mutation and a substitution of a mutant strain for a dominant strain within a host, because

658   a mutation doesn't necessarily lead to a substitution. For example, when z is (or correlates with) the

659   within-host reproductive fitness of the pathogen, substitutions would result only from mutations causing

660   an increase in z. The rate of substitution of a mutant strain $\mathbf{x}_j$ for a dominant strain $\mathbf{x}_i$, differing by a

661   single nucleotide at a locus l, is denoted $\xi_{l,i \leftarrow j}$ and defined as a function of ν, the number of alleles at the

662   locus, M_l, and the presence or absence of within-host selection with respect to z. No substitution can

663   occur between strains differing at more than one locus, although, the same effect can result from two or

664   more consecutive substitutions. Based on their scope of action, we call "within-host" the parameters ν

665   and ξ.

666   The parameters λ_{nat}, δ_{nat}, κ and ρ were kept as global constants as written in table 1.

667   The simulations were implemented as stochastic random sampling of within- and between-host events

668   (i.e. risky contact, transmission, mutation, diagnosis, death) in discrete time-steps of length 0.05

669   (arbitrary time-units). Each simulation was run for $\min(4t_{10k}, 2400)$ time-units, where t_{10k} denotes the

670   time for the simulation until reaching 10,000 diagnosed individuals. The data generated after reaching

671   10,000 diagnoses has not been used in this study but it is intended for future analysis of post-outbreak

672   dynamics, i.e. epidemic waves occurring after exhaustion of the susceptible pool. The transmission history

673   as well as the history of within-host strain substitutions was preserved during the simulations in order to

674   reproduce exact transmission trees and to extract donor and recipient values at moments of transmission

675   for the calculation of b_0.

676   *External dependencies*

677   The following third-party R-packages were used: ape v3.4 (Paradis *et al.*, 2004), data.table v1.9.6 (Dowle

678   *et al.*, 2014), adaptMCMC v1.1 (Scheidegger, 2012), Rmpfr v0.6-0 (Maechler, 2014), and coda v0.18-

679   1 (Plummer *et al.*, 2006). All programs have been run on R v3.2.4 (R Core Team, 2013).

Supplementary Material

681   Supplementary notes, figures S1-S4 and supplementary programs are available online.

Acknowledgments

References

Alizon, S., von Wyl, V., Stadler, T., Kouyos, R. D., Yerly, S., Hirschel, B., Böni, J., Shah, C., Klimkait, T., Furrer, H., Rauch, A., Vernazza, P. L., Bernasconi, E., Battegay, M., Bürgisser, P., Telenti, A., Günthard, H. F., Bonhoeffer, S., and Swiss HIV Cohort Study 2010. Phylogenetic approach reveals that virus genotype largely determines HIV set-point viral load. *PLoS pathogens*, 6(9): e1001123.

Anderson, T. J. C., Williams, J. T., Nair, S., Sudimack, D., Barends, M., Jaidee, A., Price, R. N., and Nosten, F. 2010. Inferred relatedness and heritability in malaria parasites. *Proceedings of the Royal Society B-Biological Sciences*, 277(1693): 2531–2540.

Bjorn-Mortensen, K., Soborg, B., Koch, A., Ladefoged, K., Merker, M., Lillebaek, T., Andersen, A. B., Niemann, S., and Kohl, T. A. 2016. Tracing Mycobacterium tuberculosis transmission by whole genome sequencing in a high incidence setting: a retrospective population-based study in East Greenland. *Scientific reports*, 6: 33180.

Bonhoeffer, S., Fraser, C., and Leventhal, G. E. 2015. High Heritability Is Compatible with the Broad Distribution of Set Point Viral Load in HIV Carriers. *PLoS pathogens*, 11(2): e1004634–e1004634.

Dessau, M., Goldhill, D., McBride, R. L., Turner, P. E., and Modis, Y. 2012. Selective Pressure Causes an RNA Virus to Trade Reproductive Fitness for Increased Structural and Thermal Stability of a Viral Enzyme. *PLOS Genetics*, 8(11).

Donner, A. 1986. A Review of Inference Procedures for the Intraclass Correlation Coefficient in the One-Way Random Effects Model. *International Statistical Review*, 54(1): 67–82.

Dowle, M., Short, T., Liangolou, S., and Srinivasan, A. 2014. data.table: Extension of data.frame. page 9.

Falconer, D. S. 1996. *Introduction to Quantitive Genetics*. San Val, Incorporated.

Felsenstein, J. 1988. Phylogenies And Quantitative Characters. *Annual Review of Ecology and Systematics*, 19(1): 445–471.

Fisher, R. A. 1925. *Statistical Methods For Research Workers*. Genesis Publishing Pvt Ltd.

FitzJohn, R. G. 2012. Diversitree: comparative phylogenetic analyses of diversification in R. *Methods in Ecology and Evolution*, 3(6): 1084–1092.

Fraser, C., Hollingsworth, T. D., Chapman, R., de Wolf, F., and Hanage, W. P. 2007. Variation in HIV-1 set-point viral load: epidemiological analysis and an evolutionary hypothesis. *Proceedings of the National Academy of Sciences of the United States of America*, 104(44): 17441–17446.

Fraser, C., Lythgoe, K., Leventhal, G. E., Shirreff, G., Hollingsworth, T. D., Alizon, S., and Bonhoeffer, S. 2014. Virulence and Pathogenesis of HIV-1 Infection: An Evolutionary Perspective. *Science (New York, N.Y.)*, 343(6177): 1243727–1243727.

Freckleton, R. P., Harvey, P. H., and Pagel, M. 2002. Phylogenetic analysis and comparative data: a test and review of evidence. *The American Naturalist*, 160(6): 712–726.

719 Geskus, R. B., Prins, M., Hubert, J.-B., Miedema, F., Berkhout, B., Rouzioux, C., Delfraissy, J.-F., and Meyer, L. 2007.
720 The HIV RNA setpoint theory revisited. *Retrovirology*, 4(1): 65.

721 Grimmett, G. and Stirzaker, D. 2001. *Probability and Random Processes*. Oxford University Press.

722 Hansen, T. F. 1997. Stabilizing Selection and the Comparative Analysis of Adaptation. *Evolution; international journal of*
723 *organic evolution*, 51(5): 1341–1351.

724 Hansen, T. F. and Bartoszek, K. 2012. Interpreting the evolutionary regression: the interplay between observational and
725 biological errors in phylogenetic comparative studies. *bioRxiv*, 61(3): 413–425.

726 Hartyl, D. L. and Clark, A. G. 2007. *Principles of population genetics*. Sinauer Associates.

727 Hecht, F. M., Hartogensis, W., Bragg, L., Bacchetti, P., Atchison, R., Grant, R., Barbour, J., and Deeks, S. G. 2010. HIV
728 RNA level in early infection is predicted by viral load in the transmission source. *AIDS (London, England)*, 24(7):
729 941–945.

730 Hodcroft, E., Hadfield, J. D., Fearnhill, E., Phillips, A., Dunn, D., O'Shea, S., Pillay, D., Brown, A. J. L., Database, o.
731 b. o. t. U. H. D. R., and Study, t. U. C. 2014. The Contribution of Viral Genotype to Plasma Viral Set-Point in HIV
732 Infection. *PLoS pathogens*, 10(5): e1004112.

733 Hollingsworth, T. D., Laeyendecker, O., Shirreff, G., Donnelly, C. A., Serwadda, D., Wawer, M. J., Kiwanuka, N., Nalugoda,
734 F., Collinson-Streng, A., Ssempijja, V., Hanage, W. P., Quinn, T. C., Gray, R. H., and Fraser, C. 2010. HIV-1 transmitting
735 couples have similar viral load set-points in Rakai, Uganda. *PLoS pathogens*, 6(5): e1000876.

736 Housworth, E. A., Martins, E. P., and Lynch, M. 2004. The phylogenetic mixed model. *The American Naturalist*, 163(1):
737 84–96.

738 Hu, S., Clewley, J. P., Cane, P. A., and Pillay, D. 2004. HIV-1 pol gene variation is sufficient for reconstruction of
739 transmissions in the era of antiretroviral therapy. *AIDS (London, England)*, 18(5): 719–728.

740 Jacquard, A. 1983. Heritability: One Word, Three Concepts. *Biometrics*, 39(2): 465.

741 Keele, B. F., Giorgi, E. E., Salazar-Gonzalez, J. F., Decker, J. M., Pham, K. T., Salazar, M. G., Sun, C., Grayson, T., Wang,
742 S., Li, H., Wei, X., Jiang, C., Kirchherr, J. L., Gao, F., Anderson, J. A., Ping, L.-H., Swanstrom, R., Tomaras, G. D.,
743 Blattner, W. A., Goepfert, P. A., Kilby, J. M., Saag, M. S., Delwart, E. L., Busch, M. P., Cohen, M. S., Montefiori,
744 D. C., Haynes, B. F., Gaschen, B., Athreya, G. S., Lee, H. Y., Wood, N., Seoighe, C., Perelson, A. S., Bhattacharya,
745 T., Korber, B. T., Hahn, B. H., and Shaw, G. M. 2008. Identification and Characterization of Transmitted and Early
746 Founder Virus Envelopes in Primary HIV-1 Infection. *Proceedings of the National Academy of Sciences of the United*
747 *States of America*, 105(21): 7552–7557.

748 Keeling, M. J. and Rohani, P. 2007. *Modeling Infectious Diseases in Humans and Animals*. Princeton University Press.

749 LANDE, R. 1976. Natural-Selection and Random Genetic Drift in Phenotypic Evolution. *Evolution; international journal*
750 *of organic evolution*, 30(2): 314–334.

751 Leventhal, G. E. and Bonhoeffer, S. 2016. Potential Pitfalls in Estimating Viral Load Heritability. *Trends in microbiology*.

752 Lingappa, J. R., Thomas, K. K., Hughes, J. P., Baeten, J. M., Wald, A., Farquhar, C., de Bruyn, G., Fife, K. H., Campbell,
753 M. S., Kapiga, S., Mullins, J. I., and Connie Celum, f. t. P. i. P. H. H. T. S. T. 2013. Partner Characteristics Predicting
754 HIV-1 Set Point in Sexually Acquired HIV-1 Among African Seroconverters. *www.liebertpub.com*, 29(1): 164–171.

755 Lynch, M. 1991. Methods for the Analysis of Comparative Data in Evolutionary Biology. *Evolution; international journal*
756 *of organic evolution*, 45(5): 1065–1080.

757 Lynch, M. and Walsh, B. 1998. *Genetics and Analysis of Quantitative Traits*. Sinauer Associates Incorporated.

Lythgoe, K. A. and Fraser, C. 2012. New insights into the evolutionary rate of HIV-1 at the within-host and epidemiological levels. *Proceedings: Biological Sciences*, 279(1741): 3367–3375.

Maechler, M. 2014. Rmpfr: R MPFR - Multiple Precision Floating-Point Reliable.

Mellors, J. W., Rinaldo, C. R., Gupta, P., White, R. M., Todd, J. A., and Kingsley, L. A. 1996. Prognosis in HIV-1 infection predicted by the quantity of virus in plasma. *Science (New York, N.Y.)*, 272(5265): 1167–1170.

Metzner, K. J. 2016. HIV Whole-Genome Sequencing Now: Answering Still-Open Questions. *Journal of clinical microbiology*, 54(4): 834–835.

Mitov, V. and Stadler, T. 2017. POUMM: An R-package for Bayesian Inference of Phylogenetic Heritability.

Paradis, E., Claude, J., and Strimmer, K. 2004. APE: Analyses of Phylogenetics and Evolution in R language. *Bioinformatics*, 20(2): 289–290.

Plummer, M., Best, N., Cowles, K., and Vines, K. 2006. CODA: Convergence Diagnosis and Output Analysis for MCMC. *R News*, 6: 7–11.

Presloid, J. B., Mohammad, T. F., Lauring, A. S., and Novella, I. S. 2016. Antigenic diversification is correlated with increased thermostability in a mammalian virus. *Virology*, 496: 203–214.

R Core Team 2013. R: A Language and Environment for Statistical Computing.

Scheidegger, A. 2012. adaptMCMC: Implementation of a generic adaptive Monte Carlo Markov Chain sampler.

Shirreff, G., Alizon, S., Cori, A., Günthard, H. F., Laeyendecker, O., van Sighem, A., Bezemer, D., and Fraser, C. 2013. How effectively can HIV phylogenies be used to measure heritability? *Evolution, Medicine, and Public Health*, 2013(1): 209–224.

Tang, J., Tang, S., Lobashevsky, E., Zulu, I., Aldrovandi, G., Allen, S., Kaslow, R. A., and Zambia-UAB HIV Research Project 2004. HLA allele sharing and HIV type 1 viremia in seroconverting Zambians with known transmitting partners. *AIDS research and human retroviruses*, 20(1): 19–25.

Uhlenbeck, G. E. and Ornstein, L. S. 1930. On the Theory of the Brownian Motion. *Physical Review*, 36(5): 823–841.

van der Kuyl, A. C., Jurriaans, S., Pollakis, G., Bakker, M., and Cornelissen, M. 2010. HIV RNA levels in transmission sources only weakly predict plasma viral load in recipients. *AIDS (London, England)*, 24(10): 1607–1608.

Vihola, M. 2012. Robust adaptive Metropolis algorithm with coerced acceptance rate. *Statistics and Computing*, 22(5): 997–1008.

Virgin, H. W., Wherry, E. J., and Ahmed, R. 2009. Redefining Chronic Viral Infection. *Cell*, 138(1): 30–50.

Wright, S. 1934. The Method of Path Coefficients. *The Annals of Mathematical Statistics*, 5(3): 161–215.

Yue, L., Prentice, H. A., Farmer, P., Song, W., He, D., Lakhi, S., Goepfert, P., Gilmour, J., Allen, S., Tang, J., Kaslow, R. A., and Hunter, E. 2013. Cumulative impact of host and viral factors on HIV-1 viral-load control during early infection. *Journal of Virology*, 87(2): 708–715.